ISSN 1062-8738, Bulletin of the Russian Academy of Sciences: Physics, 2024, Vol. 88, Suppl. 3, pp. S313–S321. © Pleiades Publishing, Ltd., 2024.

Laser-Driven Steering of Liquid Flows in Sessile Droplets

A. V. Dyshlyuk[a, b, *] (ORCID: 0000-0001-5804-6579)

[a] *Institute of Automation and Control Processes, Far Eastern Branch, Russian Academy of Sciences, Vladivostok, 690041 Russia*

[b] *Vladivostok State University, Vladivostok, 690041 Russia*

**e-mail: anton_dys@iacp.dvo.ru*

Received October 31, 2024; revised November 15, 2024; accepted November 28, 2024

Abstract—We studied excitation of fluid flows in sessile liquid droplets by short laser pulses. It is shown that the observed flows are Marangoni thermal flows caused by the temperature gradient of the surface tension coefficient and are excited due to the thermal effect of laser pulses on the liquid in the droplet. The cases of pinned and unpinned contact line, as well as different contact angles and different localization of the irradiating laser pulse within the droplet are investigated. The possibilities of both excitation of internal vortex flows in a stationary droplet and movement of the entire droplet on the substrate are demonstrated. The proposed technique can find application to speed up mixing of multicomponent droplets, as an additional mechanism for tailoring liquid flows in evaporating droplets to control the distribution of impurities deposited on the substrate after droplet drying, as well as for laser-assisted control of droplet motion on superhydrophobic substrates in microfluidics and lab-on-chip systems.

Keywords: thermal Marangoni effect, sessile droplets, laser induced heating, liquid flow, microfluidics, lab-on-chip

DOI: 10.1134/S1062873824709747

INTRODUCTION

In recent years, the problem of controlling internal flows in liquid droplets, as well as the movement of the entire droplet as a whole on a substrate, including on superhydrophobic surfaces [1], has attracted increased attention from researchers due to the rapid development of chemical diagnostics technologies, microfluidics systems, the creation of state-of-the-art lab-on-chip systems for solving problems in biochemistry, medicine, food industry, as well as for combating man-made and other threats to the society [2–8]. Among various types of external influences used to control the flow of liquid, such as electricity [9], magnetism [10], sound [11], heat [12], mechanical stress [13] and light [14], the latter option seems to be one of the most promising due to the widespread availability of advanced and affordable lasers which provide the ultimate concentration of electromagnetic energy in space, time and in frequency domain. Such properties of laser light as monochromaticity, directivity, spatial and temporal coherence, brightness, tight focusing capability, amplitude and frequency stability, as well as the ability to achieve extremely high intensities—both in CW and pulsed modes—provide unprecedented flexibility and a wealth of opportunities when using laser radiation to control the processes in liquid media, including liquid droplets [15–18].

Highly efficient control of liquid motion can be achieved using the Marangoni effect, which consists of inducing a liquid flow in the near-surface layer due to the gradient of the surface tension coefficient [19, 20]. Of the two varieties of the Marangoni effect—solutal Marangoni flow, which occurs when mixing liquids with different surface tension coefficients, and thermal Marangoni flow, which results from the temperature dependence of the surface tension coefficient of a single-component liquid, the thermal Marangoni effect is the option of choice for controlling liquid motion due to the simplicity of creating the required temperature distribution using pulsed or CW laser radiation acting either directly on the liquid or on a substrate in contact with a transparent liquid.

The aim of this work is to study the details of the liquid motion—both flows inside a stationary sessile droplet and the movement of the entire droplet along the substrate—due to the thermal Marangoni effect, which occurs because of controlled thermal action of pulsed laser radiation on the liquid in the droplet.

METHODOLOGY OF THE STUDY

The liquid flow is governed by a set of well-known Navier–Stokes equations, which in their most general

form are written as follows [21, 22]. The continuity equation representing conservation of mass:

$$\frac{\partial \rho}{\partial t} + \nabla \cdot (\rho \mathbf{u}) = 0,$$

vector equation for the conservation of momentum:

$$\rho \frac{\partial \mathbf{u}}{\partial t} + \rho(\mathbf{u} \cdot \nabla)\mathbf{u} = \nabla \cdot [-p\mathbf{I} + \mathbf{K}] + \mathbf{F},$$

and equation for the conservation of energy, formulated in terms of temperature:

$$\rho C_p \left(\frac{\partial T}{\partial t} + (\mathbf{u} \cdot \nabla)T\right) = -(\nabla \cdot \mathbf{q}) + \mathbf{K} : \mathbf{S} - \frac{T}{\rho}\frac{\partial \rho}{\partial T}\bigg|_p \times \left(\frac{\partial p}{\partial t} + (\mathbf{u} \cdot \nabla)p\right) + Q,$$

where ρ is the density, $\mathbf{u}$ is the velocity vector, p is pressure, $\mathbf{I}$ is the identity matrix, $\mathbf{K}$ is the viscous stress tensor, $\mathbf{F}$ is the volume force vector, C_p is the specific heat capacity at constant pressure, T is the absolute temperature, $\mathbf{q}$ is the heat flux vector, $\boldsymbol{Q}$ contains the heat sources, and $\mathbf{S}$ is the strain-rate tensor:

$$\mathbf{S} = \frac{1}{2}(\nabla \mathbf{u} + (\nabla \mathbf{u})^T),$$

and symbol "**:**" denotes the double dot product according to:

$$\mathbf{a} : \mathbf{b} = \sum_n \sum_m a_{nm} b_{nm}.$$

The liquid of the droplet under study is Newtonian, which allows us to use the following constitutive relation:

$$\mathbf{K} = 2\mu\mathbf{S} - \frac{2}{3}\mu(\nabla \cdot \mathbf{u})\mathbf{I},$$

where μ is the dynamic viscosity.

To simplify the solution of the Navier–Stokes equations let us assume the temperature variation of the liquid density under the action of moderate power laser pulses to be insignificant and the liquid to be incompressible. This permits us to set ρ = const and recast the first two Navier–Stokes equations—using the above constitutive relation—in a more manageable, simplified form:

$$\rho \nabla \cdot \mathbf{u} = 0, \quad \rho \frac{\partial \mathbf{u}}{\partial t} + \rho(\mathbf{u} \cdot \nabla)\mathbf{u} = \nabla \cdot [-p\mathbf{I} + \mu(\nabla \mathbf{u} + (\nabla \mathbf{u})^T)] + \mathbf{F}.$$

In this work, we solve the Navier-Stokes equations numerically by the finite element method on a nonuniform mesh of triangular elements (Fig. 1a) in the time domain. Although simplified two-dimensional geometry is used to facilitate modeling, the results obtained are also indicative of the liquid flow in an axisymmetric three-dimensional drop. A rigorous generalization of the results obtained to the full three-dimensional geometry is the subject of further work.

In our calculations, we will assume that the drop being modeled is so small that gravity has no appreciable effect on its surface shape and the latter is completely determined by surface tension forces. The droplet can then be regarded to have (initially, at $t = 0$) the form of a spherical segment with a given value of the contact angle. The modeling domain corresponding to the liquid in the droplet has two boundaries: the free surface of the droplet and the interface between the liquid and the substrate. The following boundary conditions are imposed on the free surface of the droplet:

$$\mathbf{n}_i \cdot \tau_1 = -p_{\text{ext}}\mathbf{n}_i + \mathbf{f}_{\text{st}}, \quad \mathbf{u}_{\text{mesh}} = \left(\mathbf{u}_1 \cdot \mathbf{n}_i - \frac{M_{\text{f}}}{\rho_1}\right)\mathbf{n}_i,$$

where $\mathbf{u_1}$ is the fluid velocity, $\mathbf{u_{mesh}}$ is the velocity of the mesh at the liquid surface, $\mathbf{n_i}$ is the normal of the interface, M_{f} is the mass flux across the interface and $\mathbf{f_{st}}$—surface tension force:

$$\mathbf{f}_{\text{st}} = \sigma(\nabla_s \cdot \mathbf{n}_i)\mathbf{n}_i - \nabla_s \sigma,$$

where ∇_s is the surface gradient operator and σ is the surface tension coefficient.

For the interface between the liquid and substrate we use the 'wall' boundary condition implying zero liquid velocity across the boundary: $\mathbf{u} \cdot \mathbf{n_{wall}} = 0$. To consider the possibility of liquid at the wall to flow along the wall, albeit with friction, Navier slip boundary condition is imposed upon the tangential component of $\mathbf{u}$ by using the following tangential stress:

$$\mathbf{K}_{\text{nt}} = -\frac{\mu}{\beta}\mathbf{u}_{\text{slip}},$$

where $\mathbf{K}_{\text{nt}} = \mathbf{K}_{\text{n}} - (\mathbf{K}_{\text{n}} \cdot \mathbf{n}_{\text{wall}}) \cdot \mathbf{n}_{\text{wall}}$, $\mathbf{K}_{\text{n}} = \mathbf{K} \cdot \mathbf{n}_{\text{wall}}$, and $\mathbf{K}$ is the viscous stress tensor. β is a slip length, and $\mathbf{u}_{\text{slip}} = \mathbf{u} - (\mathbf{u} \cdot \mathbf{n}_{\text{wall}})\mathbf{n}_{\text{wall}}$ is the velocity tangential to the wall. Rather than setting the tangential velocity to zero (no slip boundary condition), this boundary condition sets the extrapolated tangential velocity to 0 at some reasonable distance β outside the wall.

For demonstration, we chose water as the liquid of the droplet with $\mu = 0.001$ Pa s at $T = 20°C$. The effect of the laser pulse on the liquid is modeled by an initial distribution of increased temperature in each place within the droplet. This distribution is chosen depending on whether the laser pulse is assumed to be effectively absorbed by the liquid itself, or the liquid is transparent, and the pulse is absorbed by the substrate which then heats the adjacent liquid as exemplified in Fig. 1a. In any case, laser pulse is supposed to be of moderate power so as not to cause the heating of the liquid above the boiling point. The driving force for the liquid flow caused by the laser pulse is the surface tension gradient arising from nonuniform distribution of temperature on the droplet surface combined with the temperature dependence of the surface tension

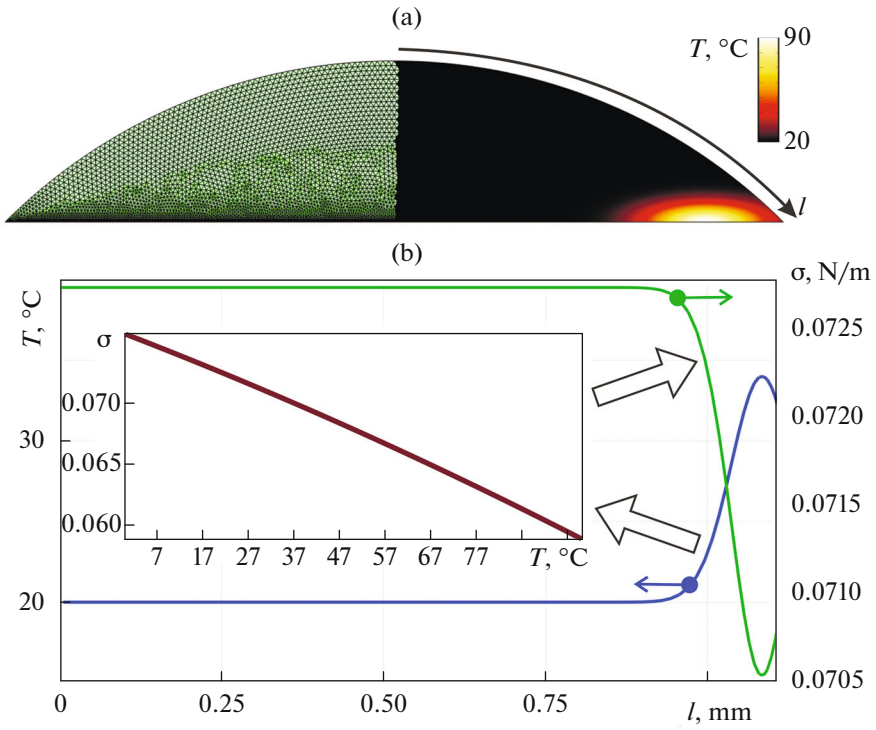

Fig. 1. (a) The liquid droplet being modelled: the computational mesh of triangular elements for the numerical solution of the Navier–Stokes equations is shown on the left-hand side, and an example of the temperature distribution induced by the irradiating laser pulse absorbed by the substrate is shown on the right-hand side, (b) the distribution of temperature on the droplet surface and the corresponding distribution of surface tension coefficient; shown in the inset is the $\sigma(T)$ dependence.

coefficient (thermal Marangoni effect) as detailed in Fig. 1b.

RESULTS AND DISCUSSION

In this paper, we investigate the dynamics of laser-induced liquid flow in droplets with three contact angles: $\alpha = 45°$, 90°, 150° and the contact line both pinned and unpinned. In all cases, we consider the situations of the droplet being irradiated by a laser pulse from above—in the center and on the edge of the droplet. To have a more pronounced effect on the droplet the laser pulse is hereinafter assumed to be effectively absorbed by the water, which in practice is readily achieved either by dyeing the water or choosing the wavelength of the pulse to match one of the water absorption bands. For the sake of demonstration clarity, we also suppose that the liquid is heated by the pulse uniformly along the pulse propagation direction and has a transverse gaussian distribution mimicking that of a typical laser pulse intensity.

Figure 2 shows the calculated time dynamics of liquid flow in the water droplet with radius $R = 1$ mm, $\alpha = 90°$ (pinned contact line) irradiated with a laser pulse (1/e spot radius 0.25 mm), propagating from above along the droplet symmetry axis. The temperature distribution T, °C (on the right) and the liquid flow velocity u, m/s (on the left) at various times are shown in different colors on the two halves of the droplet.

As can be seen from the figure, due to the symmetry of the initial distribution of elevated temperature, the liquid motion pattern is also symmetrical and represents two vortex flows, spinning clockwise (on the right) and counterclockwise (on the left). These flows arise because of the liquid movement from the region of high temperature and lower surface tension coefficient at the top of the droplet in both directions down its surface to colder regions with a higher value of σ. These flows relax in a time of about 0.2 s, which is accompanied by the equalization of temperature throughout the volume of the droplet—due to the diffusion of heat and intensive mixing of the liquid—with a deviation from the average value of +/– ~1°C. The liquid flow velocity reaches a maximum value of ~0.5 m/s approximately 10 ms after the drop is irradiated with a laser pulse.

When the droplet is irradiated by a pulse on the edge (Fig. 3), the liquid flow also has a vortex character, but due to the breaking of the left-right symmetry, the vortex is localized only on one side of the drop—the one opposite to where the laser pulse heats the liquid. The quantitative characteristics of the vortex flow

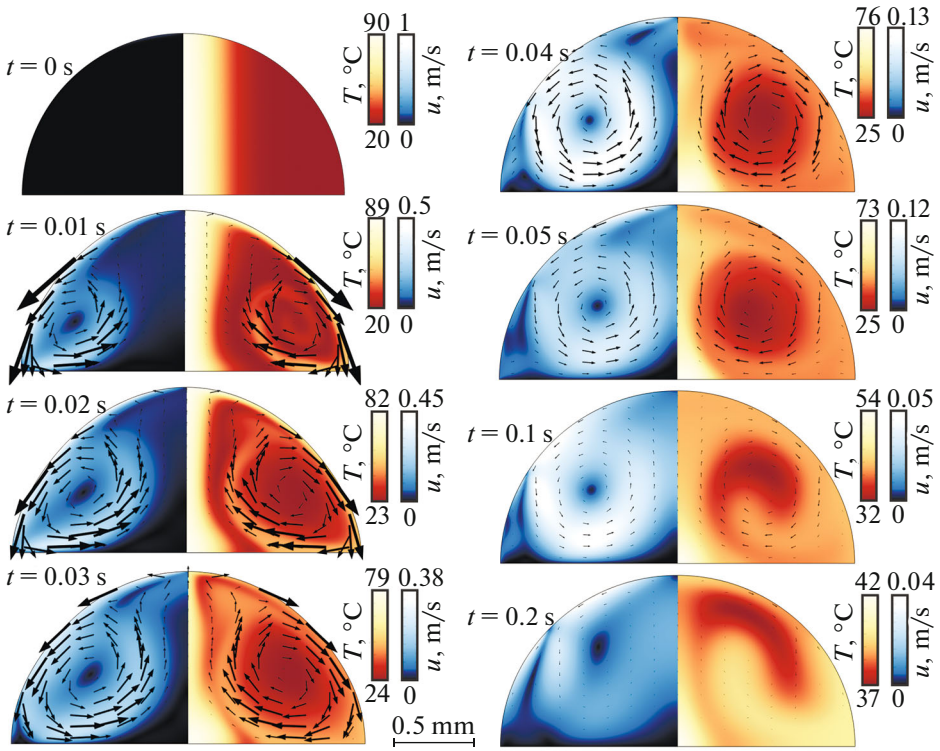

Fig. 2. Temporal evolution of the liquid flow in the sessile droplet induced by a laser pulse with spot radius 0.25 mm incident from above along the symmetry axis of the droplet and absorbed by the liquid. The contact angle is $\alpha = 90°$ and the contact line is assumed pinned. Shown with different color schemes are the temperature distribution T, °C (on the right) and the liquid flow velocity u, m/s (on the left). Note the different scales of the color schemes at various times as indicated by the color legends.

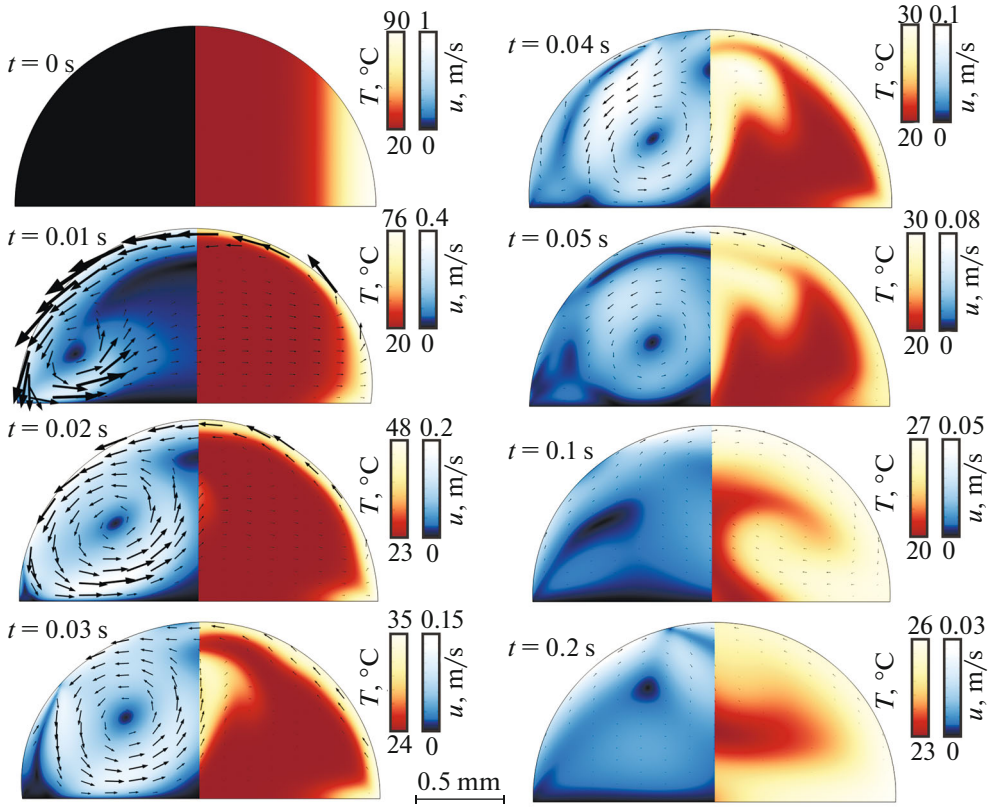

Fig. 3. Temporal evolution of the liquid flow in the droplet induced by a laser pulse incident from above on the edge of the droplet. The contact angle is $\alpha = 90°$ and the contact line is assumed pinned.

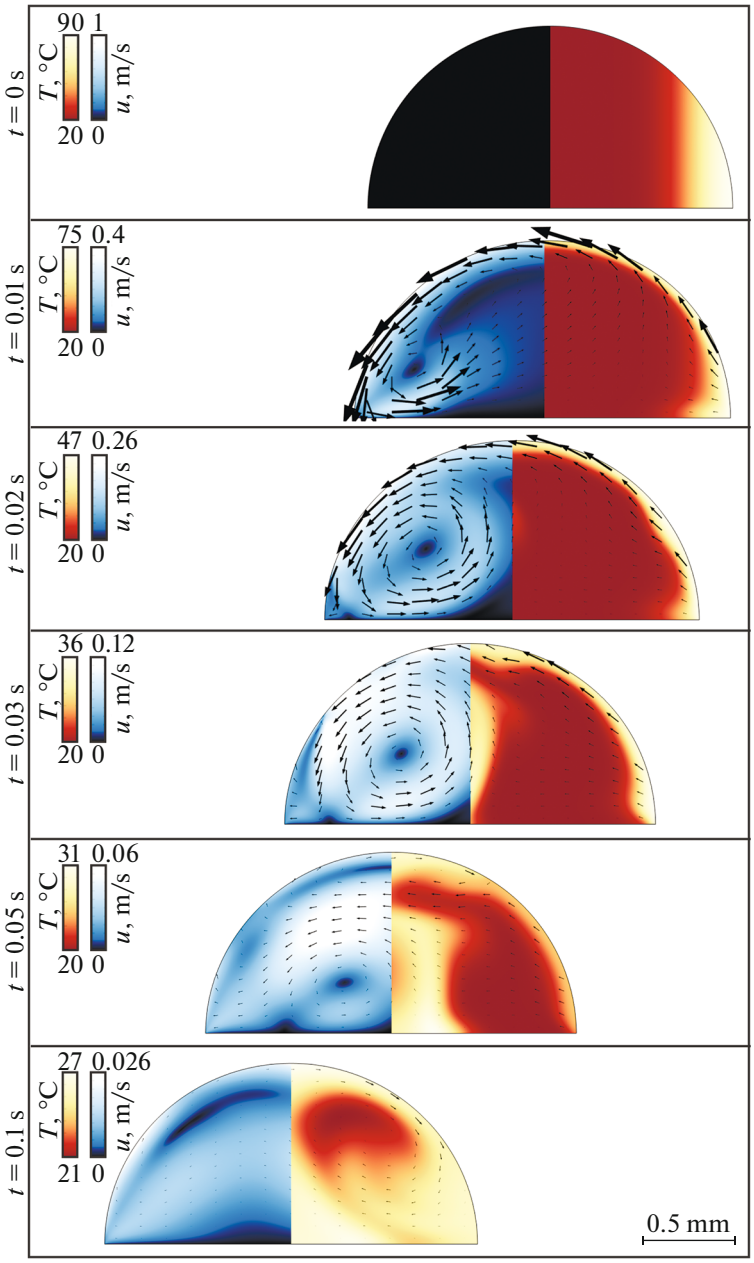

Fig. 4. Temporal evolution of the liquid flow and the movement of the entire droplet as a whole induced by a laser pulse incident from above on the edge of the droplet with unpinned contact line ($\alpha = 90°$).

in this case are like those of the central irradiation of the droplet.

Upon careful examination of Figs. 2 and 3, it can be noticed that the flow of liquid in the droplet is accompanied by slight oscillatory movements of the surface of the droplet, however the droplet does not move due to the pinned contact line. Figure 4 shows the results of modeling the flow of liquid in a droplet with an unpinned contact line and irradiation from the edge.

As can be seen, in the case when the droplet can move freely along the surface, part of the momentum of the liquid flow moving from right to left inside the droplet is transferred to the entire droplet as a whole and it moves a distance of ~R in a time of ~0.1 s (the average speed of movement is thus ~10 cm/s), which is accompanied by an approximately twofold increase in the relaxation rate of the internal flows.

The results of studying the liquid flows induced by a laser pulse in a droplet with an obtuse contact angle are shown in Fig. 5 (pinned contact line, irradiation at the center), Fig. 6 (pinned contact line, irradiation from the edge) and Fig. 7 (unpinned contact line, irradiation from the edge). It is evident from the figures that in a droplet with an obtuse contact angle and

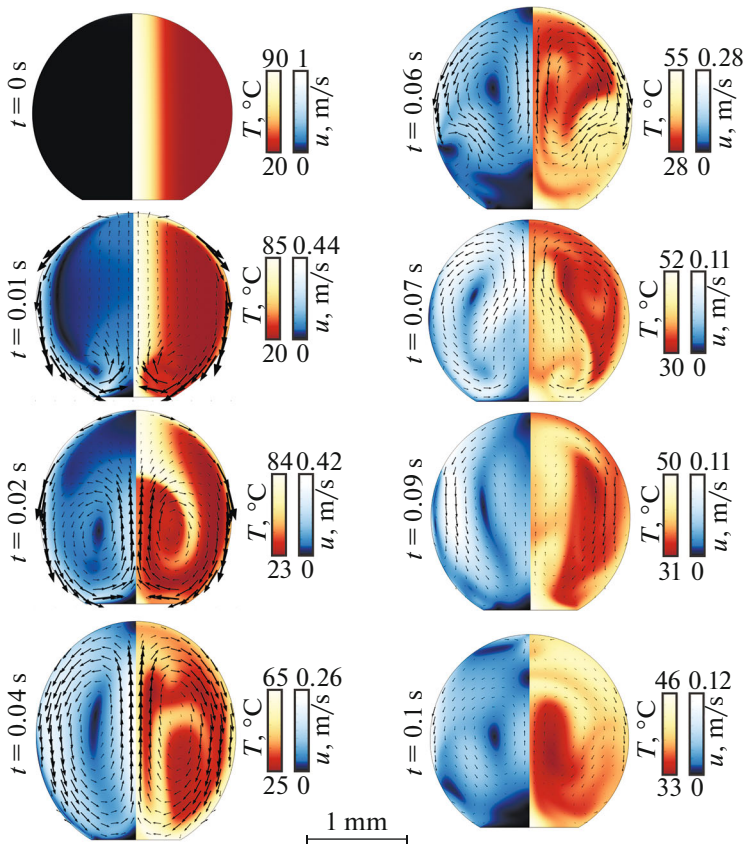

Fig. 5. Temporal evolution of the liquid flow induced by a laser pulse incident from above at the center of the droplet with an obtuse contact angle $\alpha = 150°$ and pinned contact line.

pinned contact line, the oscillations of the surface accompanying internal liquid flows are more pronounced. More complex dynamics of the internal liquid flows are also observed both with central and peripheral irradiation. In the case of an unpinned contact line, the entire droplet moves again along the substrate, but over a greater distance (~2.5R) and with a higher average speed (12.5 m/s) than at $\alpha = 90°$. Note also that the droplet moves in this case in the opposite direction—in the direction from which the laser pulse heats the droplet. This fact is explained by the rounded surface of the droplet, which significantly changes the conditions for the transfer of the internal liquid flow momentum to the entire droplet.

For comparison, we show in Fig. 8 the results of flow simulation in a droplet with an acute contact angle of $\alpha = 45°$: with central irradiation and unpinned contact line (Fig. 8a), with peripheral irradiation and pinned contact line (Fig. 8b). As can be seen from the figures, the liquid flow with central irradiation is accompanied by significant flattening of the droplet shape and increasing the size of the contact area. A tendency towards droplet rupture is evident, which can be achieved by properly selecting parameters of the irradiating laser pulse and corresponding distribution of the elevated temperature it creates [23]. The pattern of internal flows after relaxation of the drop surface oscillations is like that with $\alpha = 90°$, but the characteristic times of hydrodynamic processes are approximately an order of magnitude shorter. With lateral irradiation, significant changes in the droplet shape are also observed on short time scales on the order of milliseconds, however, are asymmetric because of the left-right symmetric breaking.

CONCLUSIONS

Thus, in this work we have investigated the temporal dynamics of liquid flows in a sessile droplet irradiated by a laser pulse heating the liquid in the droplet. It has been shown that due to the temperature gradient of the surface tension coefficient near the droplet surface a liquid flow develops from the region of higher temperature to the region of lower temperature, which evolves into vortex liquid flows inside the droplet. The configuration of these flows depends on the contact angle α of the droplet, the localization of the region of elevated temperature inside the droplet, and whether the contact line is pinned or not. When the contact line is pinned, the internal flows are accompanied by oscillations of the droplet surface of varying intensity on characteristic time scales from a few to some ten

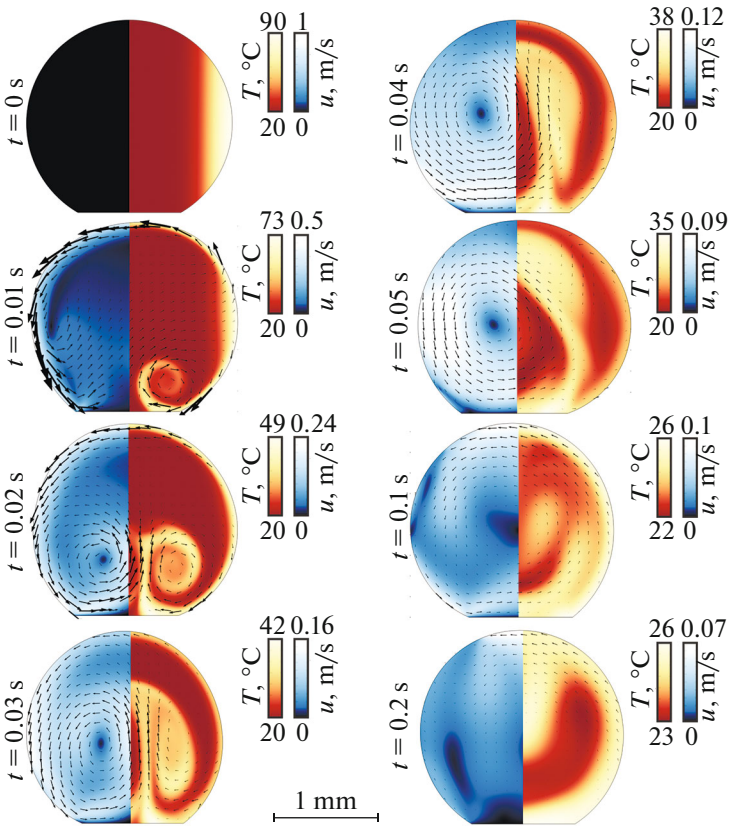

Fig. 6. Temporal evolution of the liquid flow induced by a laser pulse incident from above on the edge of the droplet with an obtuse contact angle $\alpha = 150°$ and pinned contact line.

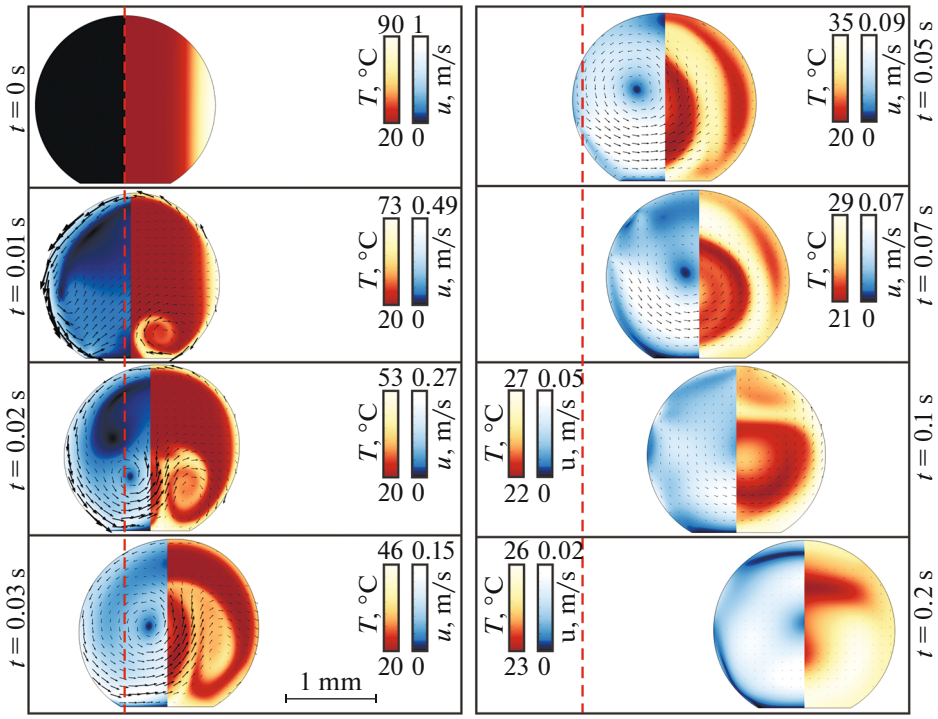

Fig. 7. Temporal evolution of the liquid flow and the movement of the entire droplet induced by a laser pulse incident on the edge of the droplet with unpinned contact line and obtuse contact angle $\alpha = 150°$.

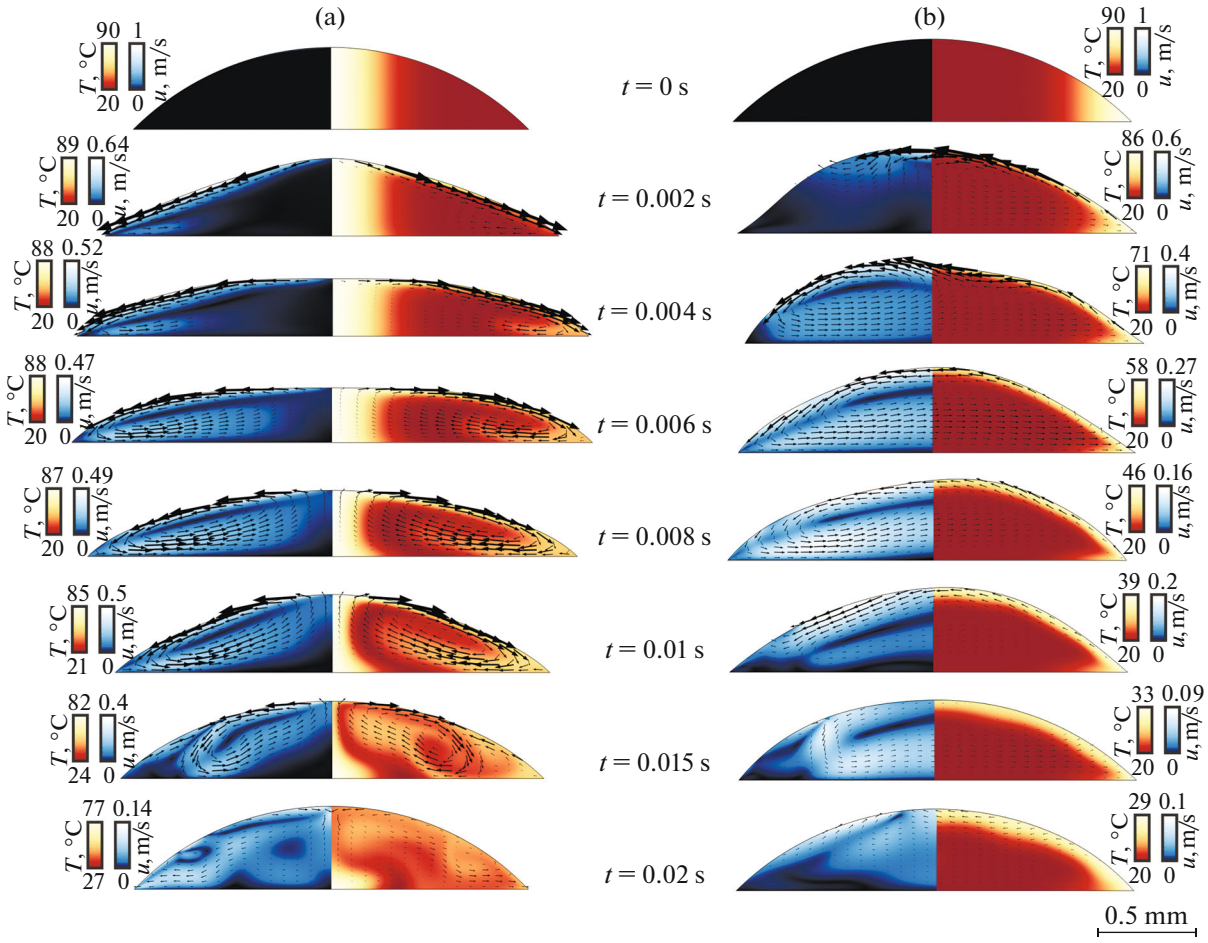

Fig. 8. (a) Temporal evolution of the liquid flow and deformation of the droplet induced by a laser pulse incident from above at the center of the droplet with unpinned contact line and acute contact angle $\alpha = 45°$. (b) Temporal evolution of the liquid flow and deformation of the droplet induced by a laser pulse incident from above at the center of the droplet with pinned contact line and acute contact angle $\alpha = 45°$.

milliseconds depending on the value of α and the location of the heated region. When the contact line is unpinned, liquid flows inside the droplet can lead to both flattening of the droplet with a significant increase in contact area, as was shown in the example of the droplet with $\alpha = 45°$, and to the movement of the droplet on the substrate. The latter occurs most efficiently at an obtuse contact angle at $\alpha = 150°$, the droplet movement over 2.5 mm with an average speed of 12.5 cm/s was demonstrated. The results obtained in the work can find practical applications in chemical analysis and medical diagnostics—for rapid mixing of liquid in multicomponent droplets, for the implementation of laser-controlled movement of droplets on superhydrophobic substrates, including lab-on-chip systems. The demonstrated effects can also be used as an additional mechanism for controlling liquid flows in evaporating droplets to tailor the distribution of impurity deposits on the substrate after total drying of the droplet.

FUNDING

The presented study is performed within the state task of the Institute of Automation and Control Processes, Far Eastern Branch, Russian Academy of Sciences (project no. 121021600267-6, FWFW-2021-0001).

CONFLICT OF INTEREST

The author of this work declares that he has no conflicts of interest.

REFERENCES

1. Yang, C., Zeng, Q., Huang, J., et al., *Adv. Colloid Interface Sci.*, 2022, vol. 306, p. 102724.
2. Yang, Y., Jiang, P., Li, H., Li, W., Li, D., Yan, X., Zhu, X., Ye, D., Yang, Y., Wang, H., Chen, R., and Liao, Q., *J. Phys. Chem. Lett.*, 2024, vol. 15, no. 34, p. 8877.

3. Dak, P., Ebrahimi, A., Swaminathan, V., Duarte-Guevara, C., Bashir, R., and Alam, M.A., *Biosensors*, 2016, vol. 6, no. 2, p. 14.
4. Leman, M., Abouakil, F., Griffiths, A.D., and Tabeling, P., *Lab Chip*, 2015, vol. 15, no. 3, p. 753.
5. Han, K., Wang, Z., Han, X., Wang, X., Guo, P., Che, P., Heng, L., and Jiang, L., *Adv. Funct. Mater.*, 2022, vol. 32, no. 45, p. 2207738.
6. Pavliuk, G.P., Zhizhchenko, A.Y., and Vitrik, O.B., *Bull. Russ. Acad. Sci.: Phys.*, 2023, vol. 87, no. 3, p. 429.
7. Lesev, V.N. and Sozaev, V.A., *Bull. Russ. Acad. Sci.: Phys.*, 2016, vol. 80, p. 689.
8. Inogamov, N.A., Zhakhovsky, V.V., and Khokhlov, V.A., *JETP Lett.*, 2022, vol. 115, no. 1, p. 16.
9. Li, Y., Li, J., Liu, L., Yan, Y., Zhang, Q., Zhang, N., He, L., Liu, Y., Zhang, X., Tian, D., Leng, J., and Jiang, L., *Adv. Sci.*, 2020, vol. 7, no. 18, p. 2000772.
10. Kim, D. and Lee, J.B., *J. Korean Phys. Soc.*, 2015, vol. 66, p. 282.
11. Naka, M. and Hasegawa, K., *Phys. Fluids*, 2020, vol. 32, no. 12.
12. Mitsunobu, M., Kobayashi, S., Takeyasu, N., and Kaneta, T., *Anal. Sci.*, 2017, vol. 33, no. 6, p. 709.
13. Jiao, Y., Zhang, Y., Lv, X., Ji, J., Wang, Z., Su, Y., Liu, X., and Liu, K., *Langmuir*, 2021, vol. 37, no. 6, p. 2140.
14. Lorenz, R.M., Edgar, J.S., Jeffries, G.D., and Chiu, D.T., *Anal. Chem.*, 2006, vol. 78, no. 18, p. 6433.
15. He, X., Elmer, J.W., and DebRoy, T., *J. Appl. Phys.*, 2005, vol. 97, no. 8.
16. Rivière, D., Selva, B., Chraibi, H., Delabre, U., and Delville, J.P., *Phys. Rev. E*, 2016, vol. 93, no. 2, p. 023112.
17. Delville, J.P., de Saint Vincent, M.R., Schroll, R.D., Chraibi, H., Issenmann, B., Lasseux, D., Zhang, W.W., Brasselet, E., Chraibi, H., and Wunenburger, R., *J. Opt. A: Pure Appl. Opt.*, 2009, vol. 11, no. 3, p. 034015.
18. Wang, Y., Zhang, Q., Zhu, Z., Lin, F., Deng, J., Ku, G., DongS., Song, S., Alam, Md. K., Liu, D., Wang, Z., and Bao, J., *Sci. Adv.*, 2017, vol. 3, no. 9, p. e1700555.
19. *Interfacial Phenomena and the Marangoni Effect*, Velarde, M.G., and Zeytounian, R.K., Eds., New York: Springer, 2002.
20. Hu, H., and Larson, R.G., *J. Phys. Chem. B*, 2006, vol. 110, no. 14, p. 7090.
21. Panton, R.L., *Incompressible Flow*, Hoboken: Wiley, 1996, 2nd ed.
22. Bird, R.B., Stewart, W.E., and Lightfoot, E.N., *Transport Phenomena*, Hoboken: Wiley, 2007, 2nd ed.
23. Li, W., Li, D., Wang, Y., Zhu, X., Ye, D., Yang, Y., Wang, H., Chen, R., and Liao, Q., *J. Phys. Chem. Lett.*, 2023, vol. 14, no. 32, p. 7313.